Micro-CT studies on 3-D bioactive glass-ceramic scaffolds for bone regeneration.

Chiara Renghini[a,b,c], Vladimir Komlev[a,d], Fabrizio Fiori[a,b,c], Enrica Verné[e], Francesco Baino[e,*],

Chiara Vitale-Brovarone[e]

[a] *Department SAIFET - Section of Physical Sciences, Polytechnic University of Marche, Ancona, Italy*

[b] *INBB – Istituto Nazionale Biostrutture e Biosistemi, Italy.*

[c] *CNISM – Matec, Ancona, Italy.*

[d] *Institute for Physical Chemistry of Ceramics, Russian Academy of Sciences, Moscow, Russia.*

[e] *Department of Materials Science and Chemical Engineering, Politecnico di Torino, Italy.*

*Corresponding author: Francesco Baino

Tel.: +39 011 5644708

Fax: + 39 011 5644699

E-mail address: francesco.baino@polito.it

Abstract

The aim of this study is the preparation and characterization of bioactive glass-ceramic scaffolds for bone tissue engineering. At this purpose, a glass belonging to the system SiO_2-P_2O_5-CaO-MgO-Na_2O-K_2O (CEL2) was used. The sponge replication method was adopted to prepare the scaffolds; specifically, a polymeric skeleton was impregnated with a slurry containing CEL2 powders, polyvinyl alcohol (PVA) as binding agent and distilled water. The impregnated sponge was then thermally treated to remove the polymeric phase and to sinter the inorganic one. The obtained scaffolds possessed an open and interconnected porosity, analogous to cancellous bone texture and mechanical strength above 2 MPa. Moreover, the scaffolds underwent a partial bioresorption due to ion-leaching phenomena. This feature was investigated by X-ray computed microtomography (micro-CT). Micro-CT is a 3D radiographic imaging technique, able to achieve a spatial resolution close to 1 μm^3. The use of synchrotron radiation allows to tune the selected photon energy to optimize the contrast among the different phases in the investigated samples. The 3D scaffolds were soaked in a simulated body fluid (SBF) to study the formation of hydroxyapatite (HAp) microcrystals on the scaffold struts and on the internal pore walls. The 3D scaffolds were also soaked in a buffer solution (TRIS-HCl) for different time frames to assess the scaffold bioresorption, according to ISO standard. A gradual resorption of the pores walls was observed during the soakings both in SBF and in TRIS-HCl.

Keywords: Glass-ceramic Scaffolds; X-ray computed microtomography; Bioactivity; Bioresorption.

Introduction

During the last decade the progress in chemical, physical, material and biological sciences resulted in the possibility of bone tissue engineering, *i.e.* a biologically based method for repair and regeneration of natural tissues [1-4]. A key component in tissue engineering for bone regeneration is the scaffold, that acts as a template for cell interactions and for the growth of bone-extracellular matrix to provide structural support to the newly formed tissue [5].

Many researchers have tried to define which properties are required for an optimal synthetic scaffold, in particular for bone tissue replacement [6-14]. First of all scaffolds need to be biocompatible. A three-dimensional (3-D) internal geometry, similar to bone morphology, and the retention of mechanical properties after implantation are required for scaffolds in order to maintain a tissue space of prescribed size and shape for tissue formation. A porosity higher than 50-60%vol. seems to be necessary. In the case of ceramic scaffolds, a macroporosity of 100–500 μm is needed to promote bone cell attachment, and a microporosity of less than 10 μm should favour ion and liquid diffusion [15].

Scaffold properties depend primarily on the nature of the biomaterial, on the fabrication process [16-19] and on the implant 3-D micro-architecture. The nature of the biomaterial has been the subject of extensive studies including different materials such as metals, ceramics, glasses, chemically synthesized polymers, natural polymers and combinations of these materials to form composites. Moreover, several methods have been developed to create highly porous scaffolds, including fiber bonding [17], solvent casting/particulate leaching [20], gas foaming [19], phase separation [21], space holder technique [22,23]. Interstitial flow has been shown to have an important role in bone growth [24]. The scaffold 3-D architecture determines the level of flow inducing shear stress on cells adhered to the scaffold walls both *in vitro* (for tissues cultured in bioreactors) and *in vivo*.

The replication process to produce 3D-scaffolds presents interesting advantages. This technique involves the use of a macroporous polymeric skeleton that is impregnated with a slurry (suspension) containing the bioactive glass particles; the impregnated sponge is then thermally treated to remove the polymeric phase and to sinter the inorganic one. The optimization of the process parameters finally leads to a highly bioactive 3D-macroporous structure [25], characterized by an open and highly interconnected porosity, analogous to the one of the spongious bone [25-27]. These scaffolds can undergo a partial bioresorption due to ions leaching phenomena.

The aim of this study was to characterize bioactive and bioresorbable glass-ceramic scaffolds. In particular, microarchitectural parameters were evaluated by X-ray micro-computed tomography (micro-CT). X-ray computed microtomography is known to be a unique technique for the non-invasive, non-destructive 3-D characterization of materials in medicine, material science and biology. Micro-CT is a 3-D radiographic imaging technique, similar to conventional computed tomography (CT) systems used in medical and industrial applications. Unlike such systems, which typically have a maximum spatial resolution of about 1 mm^3, micro-CT is capable to achieve a spatial resolution of the order of 1 μm^3. In particular, synchrotron radiation offers the possibility to select X-rays with a small energy bandwidth from the wide and continuous energy spectrum and, at the same time, it guarantees a high enough photon flux for efficient imaging [28-30]. Moreover, the use of synchrotron radiation allows to tune the selected photon energy in order to optimize the contrast of the different phases in the investigated samples. This possibility sparks great interest for micro-CT since it allows high spatial resolution images to be generated from 10 to 1 μm, with high signal-to-noise ratio [31-33]. The recent use of micro-CT in scaffold research has enabled accurate morphological studies to be carried out, yielding comprehensive data sets [34-42]. Very promising and advanced fields of investigations can be opened by micro-CT in tissue engineering [43], but in most of the research works its use is limited to the visualization of the scaffold morphology and the determination of its porosity while the investigation of the newly formed phase is usually carried out only at the scaffold surface by SEM and X-ray diffraction [44-45]. Research studies reporting

In this work an accurate analysis of 3-D scaffold structure was performed, in order to confirm and extend the promising results, already showed in previous works, concerning the use of CEL2 glass-ceramic as effective biomaterial for scaffolding. In particular, micro-CT analysis is used to study the new phase 3D distribution in the bulk material and its evolution as a function of the soaking time in a simulated body fluid and TRIS-HCl medium. These results are completed by SEM and X-ray diffraction measurements.

Materials and methods

In this study, glass-ceramic macroporous scaffolds were prepared using a polyurethane (PU) sponge such as organic template and bioactive glass-ceramic powders.

The chosen glass-ceramic, belonging to the system SiO_2-P_2O_5-CaO-MgO-Na_2O-K_2O (CEL2), was already studied and characterized in previous works [23,25] due to its excellent biocompatibility and bioactivity [46], and has the following molar composition: 45% SiO_2, 3% P_2O_5, 3% , 26% CaO, 7% MgO, 15% Na_2O, 4% K_2O.

Briefly, CEL2 was prepared by melting the raw products (SiO_2, $Ca_3(PO_4)_2$, $CaCO_3$, $4MgCO_3 \cdot Mg(OH)_2 \cdot 5H_2O$, Na_2CO_3, K_2CO_3) in a platinum crucible at 1400 °C for 1 h in air and by quenching the melt in cold water to obtain a frit, that afterwards was ground by ball milling and sieved to a final grain size below 30 μm.

Scaffolds preparation

The organic template used in this work is an open-cell polyurethane sponge characterized by a highly interconnected macroporosity. The sponge was cut into 1.5 cm × 1.5 cm × 1.5 cm cubic blocks and then impregnated with a slurry containing CEL2 particles (weight composition: 25% CEL2, 6% PVA, 69% water). First PVA was hydrolyzed and stirred in distilled water at 60 °C and,

after 1 h of mixing, the glass powders were added to the solution. Then the polymeric template underwent the infiltration process: the sponge blocks were soaked in the glass slurry and taken back for several times, followed by cycles of compression to shrink the sponge in thickness along the three spatial directions, in order to remove the exceeding slurry. Afterwards the samples were thermally treated at 950 °C for 3 h (heating and cooling rate were 5 and 10 °C/min respectively) in order to remove the polymeric phase and to sinter the inorganic one, so that macroporous glass-ceramic scaffolds were produced.

The scaffolds were soaked for 1 week and for 4 weeks in 25 ml of simulated body fluid (SBF) and TRIS-HCl [47], maintained at 37 °C in polyethylene bottles and according to ISO standard [48].

The scaffolds, before and after the soaking in SBF and TRIS-HCl, were characterized by means of morphological investigations (SEM, Philips 525 M), compositional analysis (EDS, Philips EDAX 9100), X-ray diffraction analysis (Rigaku Denki diffractometer) and, specifically, X-ray computed microtomography (micro-CT).

X-ray computed microtomography

Micro-CT experiments were performed at ELETTRA (Trieste, Italy), on the beamline SYRMEP, using a monochromatic beam with an energy of 23.5 keV and a sample-to-detector distance of 5 cm. A two-dimensional (2-D) detector records projections of the sample for different angular positions, as shown in fig. 1. For the present study 1440 projections within an angular range of 180° were taken. The exposure time was 4 s per projection. The images were recorded on a 2048×2048 CCD detector, with the pixel size set to 9 μm. The 3D structure was finally reconstructed using a filtered back-projection algorithm. A volume of interest was reconstructed for each sample; a single voxel of the reconstructed image had a size of $9 \times 9 \times 9$ μm^3. The linear attenuation coefficient for the employed X-ray energy ranged between 0 and 9 cm^{-1}, distributed in 256 image gray levels.

A 2 GHz Pentium with 1 GB RAM and the commercial software VG Studio MAX 1.2. were used to generate 3-D images and to show the distribution of phases in 3-D. A scatter HQ algorithm with oversampling factor of 5.0 and activated color rendering was used in order to achieve optimal settings for the image quality.

Extraction of quantitative parameters

Quantitative analysis of the 3-D architecture was performed, based on the structural indices usually measured for bone samples [49]. All the obtained parameters and quantitative evaluations are the mean values of measurements performed on three different samples.

The scaffold volume (SV) is obtained by multiplying the number of voxels corresponding to the X-ray absorption characteristics of the scaffold material by the volume of a single voxel. The total volume (TV) is the volume occupied by all materials in the considered data set. The ratio of the scaffold surface (SS) to the scaffold volume (SV) is approximated using the Cauchy-Crofton theorem from differential geometry (it is generally not possible to calculate the scaffold surface from polygons): the mean number of crossings per unit length of randomly chosen lines through a 3-D structure approaches half of the true ratio of surface to volume [50]. Sample porosity (% vol.) can therefore be calculated as (1–SV/TV). The specific surface available for pore adhesion is given by the bone surface-to-volume ratio (SS/SV). 3-D images also enable the direct assessment of metric indices of feature sizes by actually measuring distances in the 3-D space. Trabecular (pore wall) thickness (TbTh), and trabecular separation (TbSp) or pore diameter can be computed. The trabecular thickness (TbTh) depends on SS/SV and is calculated as TbTh = 2/(BS/BV). The mean number (TbN) of trabecular structures per length unit depends on SV/TV and is calculated as TbN = (SS/SV)/TbTh. The mean space (TbSp) among trabecular structures depends on TbN and TbTh. It is calculated as TbSp = [(1/TbN) – TbTh].

Porosity was measured using IDL Virtual Machine (plug-in Blob3D). Blob3D is designed for efficient measurement of up to thousands of discrete features (*e.g.* clasts, mineral grains, porphyroblasts, voids) within a single sample [51]. Blob3D is unique because it gives the program operator primary control over data elaboration and interpretation, and all computations are carried out in 3-D, rather than individually on a series of 2-D slices.

Results and Discussion

In this study, 3-D glass ceramic scaffolds were prepared by adopting the sponge impregnation method, using an open-cells PU sponge as a template and CEL2 powders. The impregnated sponge underwent a thermal treatment at 950 °C for 3 h to allow the organic phase removal and to sinter the glass particles. The PU is completely removed at 600 °C, thus no contamination of the CEL2 scaffolds was foreseen and was actually found after sintering.

Morphological characterization

Figure 2a shows the structure of the PU open-cells sponge used as template in this work. The sponge exhibits a texture similar to spongious bone, with highly interconnected macropores ranging within 100-1000 μm. The result of the impregnation process is reported in fig. 2b. The sponge trabeculae are almost uniformly coated with CEL2 powders; some clotted pores can be observed, probably due to an incomplete removal of the exceeding slurry. As assessed by SEM investigations, the resulting scaffolds are characterized by open and interconnected macropores; for instance figure 2c shows some macropores with their struts. Moreover, a good degree of sintering, resulting in dense scaffold trabeculae, and a high porosity interconnection can be observed. The macropores size is ranging within 100-500 μm, and the pores struts thickness is about 10-50 μm. A high degree of interconnection is crucial to attain a good viability of the inner parts of the scaffold, thus

promoting a proper vascularization of the graft and an effective bone in-growth *in vivo*. A good degree of sintering and densification of the trabeculae was also achieved, in order to guarantee a structure and a mechanical strength of the implant comparable to the properties of spongious bone.

The prepared scaffolds were investigated by X-ray computed microtomography. The macroporous network and the strut microstructure of the investigated samples are illustrated in fig. 3. The 3-D model of the scaffold structure confirms that CEL2 scaffolds possess an interconnected pores network similar to trabecular bone. This result is consistent with SEM observations reported in fig. 2.

Immersion studies in SBF and in TRIS: microstructural characterization

The same 3-D scaffolds were treated in a simulated body fluid (SBF) for different time intervals in order to study the formation of hydroxyapatite crystals on the scaffold struts and on the internal pore walls. The 3-D scaffolds were also soaked in a buffered medium (TRIS-HCl) for different time intervals to assess the scaffold bioresorption with time, according to ISO standard [48].

Specifically, the study in SBF is useful to analyse the *in vitro* bioactivity of the CEL2 scaffolds, whereas the study in TRIS solution gives information about the samples bioresorbability.

The 3-D images were quantified extracting some form/geometry parameters using spatial computational analysis techniques. The results of this analysis are summarized in table 1.

An identification of phases was performed by observing 3-D images extracted from the reconstructed volumes of samples, and colouring them using the VG Studio Max 1.2. software (fig. 4 and fig. 5). A quantitative analysis of the different phases can be performed by taking into account the gray level histogram, linked to the distribution of linear absorption coefficients in the whole reconstructed volume. As shown in figure 6, both the samples in soaked SBF (fig. 6a) and those in TRIS (fig. 6b) exhibit a peak for a low gray level approximately between 80 and 125, corresponding to air, and a peak approximately between 170 and 225, corresponding to the scaffold material.

Moreover, a peak approximately between gray levels 125 and 170 appears after immersion, corresponding to the newly formed phase. This peak is evident after 4 weeks, while its presence after 1 week is masked between the other two peaks. Anyway it can be actually put into evidence by observing that the whole spectrum is well fitted by the overlap of three Pearson-7 functions, one for each phase (Fig. 6c-d). This analysis also allows the definition of the gray level thresholds mentioned above, and shows how the newly formed phase increases (the corresponding peak rises) with the soaking time. Figure 7 shows the XRD spectra of the scaffolds before (A) and after the treatments both in SBF (fig. 7a) and in TRIS (fig. 7b) for 1 week (B) and for 4 weeks (C). The diffraction patterns show that the scaffold walls are progressively covered, with the increase of soaking time in SBF and in TRIS, by a new phase layer, so that the peaks identifying the CEL2 crystalline phases are not visible after 28 days of immersion. Specifically, the formation of the hydroxyapatite (HAp) phase (broad peak at $2\theta \sim 32°$) was observed. These results are consistent both with the analysis previously reported in figure 6 and with SEM observations reported in fig. 8a-b, showing the HAp layer grown on the sample surface after immersion in SBF for 28 days, with a thickness ranging from approximately 20 to 60 μm. In fig. 8c EDS analysis, performed on the newly formed layer and confirming the presence of HAp, is reported.

Furthermore, thresholding the gray level at 170, considered (as stated above) to be the edge level between the new phase and the scaffold, it was possible to visualize the two phases separately. Figure 9 shows an example of this data treatment, performed on a sample soaked in SBF. The figures show that HAp formation starts at the periphery and progressively goes on towards the inner part of the scaffold, as already observed in figure 4.

A more accurate quantitative evaluation both of bioactivity and of bioresorption rate of the scaffolds was also performed. Considering the samples soaked in SBF, used for *in vitro* bioactivity study, the average thickness of HAp layer as a function of the immersion time was measured and the curve is reported on fig. 10. As it can be observed, with increasing immersion time there was a significant increment of the HAp layer thickness. In particular, after 4 weeks the average HAp thickness

increased to a value of almost 14.0 μm, which is comparable to SEM results (fig. 8) if one takes into account that it is an average over the whole reconstructed volume. For what concerns the bioresorption study, the scaffolds soaked in TRIS were considered. Specifically, the average thickness of scaffold walls as a function of soaking time was evaluated; these results are presented in fig. 11. In particular, after 4 weeks of immersion in TRIS the average thickness of scaffold walls decreased from 60.0 μm to a value of about 39.7 μm, but even after 1 week the porous scaffolds were already subjected to degradation.

Pore analysis

Porosity (% vol.) is defined as the percentage of void space in a solid [52] and it is a morphological property independent of the material. Pores are necessary for bone tissue formation because they allow migration and proliferation of osteoblasts and mesenchymal stem cells, as well as a proper vascularization of the implant [53]. In addition, a porous surface improves mechanical interlocking between the implant biomaterial and the surrounding natural bone, providing higher mechanical stability at this critical interface [54].

The calculated porosity, reported in table 1, shows that all the scaffolds exhibit a high percentage of porosity (about 50-60 %vol.). In particular, the total porosity slightly decreases after immersion in SBF (fig. 12a), and increases after soaking in TRIS (fig. 12b). These data are consistent with bioactivity/bioresorption studies previously exposed. The scaffold bioresorption observed in TRIS, involving a decrease of scaffold walls thickness, causes an increase of void fraction, *i.e.* pore content. On the contrary, the deposition of a HAp layer on the scaffolds soaked in SBF involves a progressive pore clotting, *i.e.* a decrease of the porosity.

A 3-D representation of the pores is showed in fig. 13 and was used to calculate the pore size distribution (fig. 14). All results demonstrate that both before and after soaking in TRIS/SBF the scaffolds exhibit a bimodal porous structure. In fact both macropores, ranging within 100-500 μm,

and micropores (size 1-100 μm), whose presence is crucial for proteins and cells adhesion, can be observed. In particular, in fig. 14b an increase of micropore amount after soaking in TRIS can be seen. This behaviour can be understood by considering the bioerosion phenomena occuring during the immersion in TRIS, in which the material bioresorption involves the formation of little pits and micropores on the scaffold walls. This is also consistent with the scaffold structure data reported in table 1, showing that a significant decrease of average pore diameter (TbSp) occurs after 4 weeks in TRIS. In fact, the increase of small micropore content, in comparison with the whole pore amount, involves the decrease of the average pore diameter.

Conclusions

In this study, 3-D highly porous scaffolds, with a trabecular texture similar to cancellous bone, were fabricated *via* sponge-replication method. The prepared scaffolds were soaked in SBF and TRIS-HCl for different time intervals and then investigated by means of X-ray micro-CT. This technique provides an excellent non-destructive way to analyse the inner structure, the total porosity, the pore size distribution and the pore morphology of scaffolds for tissue engineering. This structural characterization method is not afforded by other conventional porosity analysis techniques. Moreover, X-ray micro-CT offers a unique capability to analyse the tissue in-growth and monitor the kinetic changes occurring in pore morphology of tissue-engineering scaffolds during *in vitro* and *in vivo* tests.

Micro-CT analysis results were compared with XRD and SEM investigations. It was observed that HAp layer grew onto the samples soaked in SBF, showing the high bioactivity and biocompatibility of the glass-ceramic scaffolds. Moreover, the decrease of the mean walls thickness with the immersion time in TRIS showed the bioresorbability of the scaffolds. Finally, the porosity determined by micro-CT demonstrated that all the scaffolds, before and after the soaking in SBF and TRIS, exhibited a high percentage of porosity (50-60 %vol.). In particular, microstructural

observations revealed that the samples were characterized by a bimodal porous structure, *i.e.* macropores, necessary for the growth of new bone and the vascularization of the implant, and micropores, important for cells adhesion and proliferation. Therefore, the micro-CT analysis shows that the proposed CEL2 scaffolds are very interesting candidates for bone tissue engineering applications.

References

[1] Ma PX. Scaffolds for tissue fabrication. Materials Today 2004;7(5):30-40.

[2] Hench LL, Polak JM. Third-generation biomedical materials. Science 2002;295:1014-1017.

[3] Jones JR, Hench LL. Regeneration of trabecular bone using porous ceramics. Curr Opin in Solid State and Mater Sci 2003;7:301-307.

[4] Burg KJL, Porter S, Kellam JF. Biomaterial developments for bone tissue engineering. Biomaterials 2000;21:2347-2359.

[5] Karageorgiou V, Kaplan D. Porosity of 3D biomaterial scaffolds and osteogenesis. Biomaterials 2005;26:5474-5491.

[6] Hutmacher DW. Scaffolds in tissue engineering bone and cartilage. Biomaterials 2000;21:2529–2543.

[7] Middleton JC, Tipton AJ. Synthetic biodegradable polymers as orthopedic devices. Biomaterials 2000;21(23):2335–2346.

[8] Attawia MA, Devin JE, Laurencin CT. Immunofluorescence and confocal laser scanning microscopy studies of osteoblast growth and phenotypic expression in three-dimensional degradable synthetic matrices. J Biomed Mater Res 1995;29:843-848.

[9] Marra KG, Szem JW, Kumta PN, DiMilla PA, Weiss LE. In vitro analysis of biodegradable polymer blend/hydroxyapatite composites for bone tissue engineering. J Biomed Mater Res 1999;47:324–335.

[10] Laurencin CT, Attawia MA, Lu LQ, Borden MD, Lu HH, Gorum WJ, Lieberman JR. Poly(lactide-co-glycolide)/hydroxyapatite delivery of BMP-2-producing cells: A regional gene therapy approach to bone regeneration. Biomaterials 2001;22:1271-1277.

[11] Maquet V, Boccaccini AR, Pravata L, Notingher I, Jerome R. Porous poly(α-hydroxyacid)/Bioglass® composite scaffolds for bone tissue engineering. I: preparation and in vitro characterization. Biomaterials 2004;25:4185–94.

[12] Wang M. Developing bioactive composite materials for tissue replacement. Biomaterials 2003;24:2133–2151.

[13] Bostrom RD, Mikos AG. In: Atala A, Mooney D, editors. Synthetic biodegradable polymer scaffolds. Basel: Birkhauser; 1997. p. 215–234.

[14] Freed LE, Vunjack-Novakovic G. Culture of organized cell culture. Adv Drug Delivery Rev 1998;33(1–2):15–30.

[15] Boyan BD, Hummert TW, Dean DD, Schwartz Z. Role of material surfaces in regulating bone and cartilage cell response. Biomaterials 1996;17:137–146.

[16] Vitale-Brovarone C., Di Nunzio S., Bretcanu O., Verné E. Macroporous glass-ceramic materials with bioactive properties. J Mat Sci:Mat Med 2004;15:209-217.

[17] Mikos AG, Bao Y, Cima LG, Ingber DE, Vcanti JP, Langer R. Preparation of poly(glycolic acid) bonded fiber structures for cell attachment and transplantation. J Biomed Mater Res 1993;27:183-189.

[18] Mooney DJ, Baldwin DF, Suh NP, Vacanti JP, Langer R. Novel approach to fabricate porous sponges of poly(d,l-lactic-co-glycolic acid) without the use of organic solvents. Biomaterials 1996;17:1417-1422.

[19] Nam YS, Yoon JJ, Park TG. Novel fabrication method of macroporous biodegradable polymer scaffolds using gas foaming salt as a porogen additive. J Biomed Mater Res 2000;53:1-7.

[20] Mikos AG et al. Preparation and characterization of poly(L-lactic acid) foams. Polymer 1994;35:1068-1077.

[21] Choi YS, Hong SR, Lee YM, Song KW, Nam YS, Park TG. Studies on gelatin-containing artificial skin: II. preparation and characterization of cross-linked gelatin-hyaluronate sponge. J Biomed Mater Res 1999;48:631-639.

[22] Vitale-Brovarone C, Verné E, Borsetti M, Appendino P, Cannas M. Microstructural and in vitro characterization of SiO_2-Na_2O-CaO-MgO glass-ceramic bioactive scaffolds for bone substitutes. J Mat Sci:Mat Med 2005;16:909-917.

[23] Vitale-Brovarone C, Verné E, Robiglio L, Martinasso G, Canuto R, Muzio G. Biocompatible glass-ceramic materials for bone substitutions. J Mater Sci:Mater Med 2008;19:471-478.

[24] Knothe Tate ML. "Whither flows the fluid in bone?" An osteocyte's perspective. J Biomech 2003;36:1409-1424.

[25] Vitale-Brovarone C, Verné E, Robiglio L, Appendino P, Bassi F, Martinasso G, Muzio G, Canuto R. Development of glass-ceramic scaffolds for bone tissue engineering: Characterisation, proliferation of human osteoblasts and nodule formation. Acta Biomat 2007;3:199-208.

[26] Chen QZ, Boccaccini AR. Poly(D,L-lactic acid) coated 45S5 Bioglass [registered trademark]-based scaffolds: Processing and characterization. J Biomed Mater Res A 2006;77:445-457.

[27] Chen QZ, Thompson ID, Boccaccini AR. 45S5 Bioglass®-derived glass–ceramic scaffolds for bone tissue engineering. Biomaterials 2006;27:2414-2425.

[28] Beltrame F et al. A simple non invasive computerized method for the assessment of bone repair within osteoconductive porous bioceramic grafts. Biotech and Bioeng 2005;92(2):189-198.

[29] Marcacci M et al. Repair of large bone defects by autologous human bone marrow stromal cells. Key Eng Mater 2001;192-195:1053-1056.

[30] Kotobuki N, Ioku K, Kawagoe D, Fujimori H, Goto S, Ohgushi H. Observation of osteogenic differentiation cascade of living mesenchymal stem cells on transparent hydroxyapatite ceramics. Biomaterials 2005;26:779-785.

[31] Landis EN, Nagy EN, Keane DT. Microstructure and fracture in three dimensions. Eng Fract Mechanism 2003;70:911-925.

[32] Weyland M., Midgley P.A. Electron tomography. Materials Today 2004;7(12):32-40.

[33] Salomè M, Peyrin F, Cloetens P, Odet C, Laval-Jeantet AM, Baruchel J, Spanne P. A synchrotron radiation microtomography system for the analysis of trabecular bone samples. Med Phys 1999;26:2194-2204.

[34] Mastrogiacomo M, Komlev VS, Hausard M, Peyrin F, Turquier F, Casari S, Cedola A, Rustichelli F, Cancedda R. Synchrotron radiation microtomography of bone engineered from bone marrow stromal cells. Tissue Eng 2004;10:1767-1774.

[35] Atwood RC, Jones JR, Lee PD, Hench LL. Analysis of pore interconnectivity in bioactive glass foams using X-ray microtomography Scripta Mater 2004;51:1029-1033.

[36] Williams JM, Adewunmi A, Schek RM, Flanagan CL, Krebsbach PH, Feinberg SE, Hollister SJ, Das S. Bone tissue engineering using polycaprolactone scaffolds fabricated via selective laser sintering. Biomaterials 2005;26:4817-4827.

[37] Ho ST, Hutmacher DW. Application of micro CT and computation modeling in bone tissue engineering. Computer-Aided Design 2005;37:1151-1161.

[38] Shao XX, Hutmacher DW, Ho ST, Goh JCH, Lee EH. Evaluation of a hybrid scaffold/cell construct in repair of high-load-bearing osteochondral defects in rabbits. Biomaterials 2006;27: 1071-1080.

[39] Jones AC, Milthorpe B, Averdunk H, Limaye A et al. Analysis of 3D bone ingrowth into polymer scaffolds via micro-computed tomography imaging. Biomaterials 2004;25:4947-4954.

[40] Lin ASP, Barrows TH, Cartmell SH, Guldberg RE. Microarchitectural and mechanical characterization of oriented porous polymer scaffolds. Biomaterials 2003;24:481–489.

[41] Papadimitropoulos A., Mastrogiacomo M, Peyrin F, Molinari E., Komlev VS, Rustichelli F, Cancedda R. Kinetics of in vivo bone deposition by bone marrow stromal cells within a resorbable porous calcium phosphate scaffold: a X-ray computed microtomography study. Biotechn and Bioeng 2007; 98(1):271-281.

[42] Cancedda R, Cedola A, Giuliani A, Komlev VS, Lagomarsino S, Mastrogiacomo M, Peyrin F, Rustichelli F. Bulk and interface investigations of scaffolds and tissue engineered bones by x-ray microtomography and microdiffraction. Biomaterials 2007;28:2505-2524.

[43] Porter BD, Lin ASP, Peister A, Hutmacher D, Guldberg RE. Noninvasive image analysis of 3D construct mineralization in a perfusion bioreactor. Biomaterials 2007:28;2525-2533.

[44] Hong Z, Reis RL, Mano JF. Preparation and in vitro characterization of scaffolds of poly(l-lactic acid) containing bioactive glass ceramic nanoparticles. Acta Biomaterialia 2008 (in press).

[45] Rainer A, Giannitelli SM, Abruzzese F, Traversa E, Licoccia S, Trombetta M. Fabrication of bioactive glass–ceramic foams mimicking human bone portions for regenerative medicine. Acta Biomaterialia 2008;4(2):362-369.

[46] Vitale-Brovarone C, Baino F, Martinasso G, Canuto R, Bassi F, Verné E. Glass-ceramic scaffolds and shock waves effects on cells migration. Key Eng Mater 2008;361-363:233-236.

[47] Kokubo T, Takadama H. How useful is SBF in predicting in vivo bone bioactivity?. Biomaterials 2006;27:2907-15.

[48] ISO 10993-14:2002 standard. Biological evaluation of medical devices: identification and quantification of degradation products from ceramics.

[49] Ulrich D, Van Rietbergen B, Laib A, Ruegsegger P. Load transfer analysis of the distal radius from in-vivo high-resolution CT-imaging. J Biomech 1999;32:821–828.

[50] Parfitt AM et al. Bone Histomorphometry: Standardization of Nomenclature, Symbols, and Units. Report of the ASBMR histomorphometry nomenclature committee; 1987.

[51] Ketcham RA. The role of crystallographic angle in characterizing and modeling apatite fission-track length data. Rad Meas 2005;39:595-601.

[52] Leon y Leon CA. New perspectives in mercury porosimetry. Adv Colloid Interface Sci 1998; 76–77:341–72.

[53] Kuboki Y et al. BMP-induced osteogenesis on the surface of hydroxyapatite with geometrically feasible and nonfeasible structures: topology of osteogenesis. J Biomed Mater Res 1998;9(2):190–199.

[54] Story BJ, Wagner WR, Gaisser DM, Cook SD, Rust-Dawicki AM. In vivo performance of a modified CSTi dental implant coating. Int J Oral Maxillofac Implants 1998;13(6):749–757.

Figure

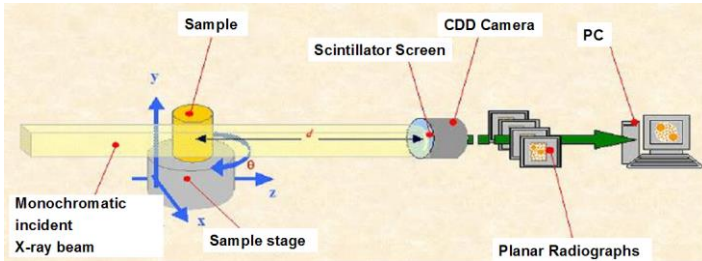Figure 1. Scheme of acquisition set-up of X-ray computed microtomography.

Figure 2. Scaffold preparation: (a) polyurethane sponge, (b) impregnated sponge and (c) scaffold structure, characterized by open and interconnected macropores.
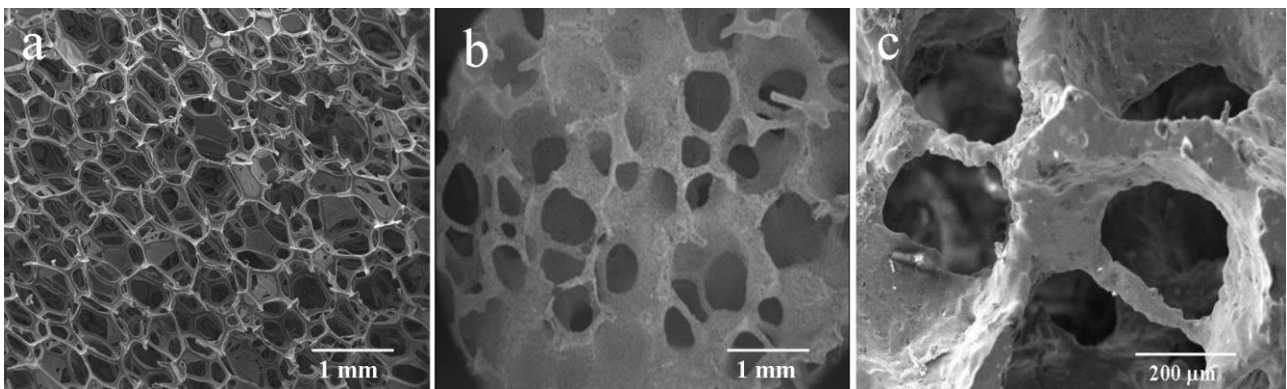

Figure 3. Macroporous network and struts microstructure of (a) the investigated samples and of (b) the sample cross-section as obtained by X-ray computed microtomography.
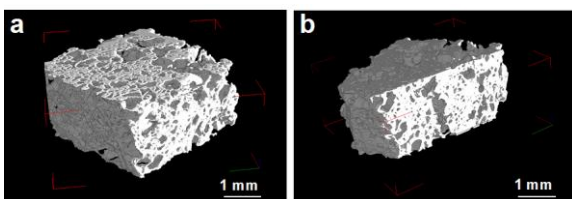
Figure 4. 3D reconstruction of scaffolds subvolume (a) before and after treatment in a SBF for (b) 1 week and for (c) 4 weeks. The image shows the scaffold (green) and the new phase (blue).
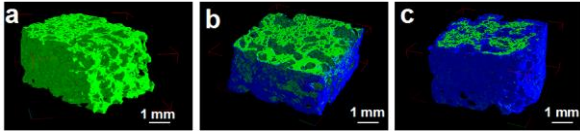
Figure 5. 3D reconstruction of scaffolds subvolume (a) before and after treatment in a buffered medium (TRIS) for (b) 1 week and for (c) 4 weeks. The image shows the scaffold (green) and the new phase (blue).
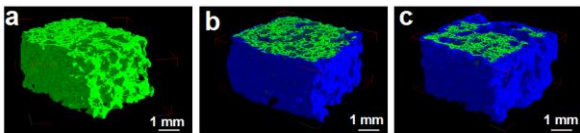
Figure 6. Gray levels analysis. Histogram of the whole reconstructed volume of the scaffolds before and after soaking in SBF (a) and TRIS (b): (A) before the treatment, (B) after 1 week, (C) after 4 weeks of immersion. The peak on the left corresponds to the air, the peak on the right corresponds to the scaffold material and the central peak corresponds to the new phase. The fitting curves of the scaffolds after soaking in SBF for 1 week (c) and 4 weeks (d) are also reported.
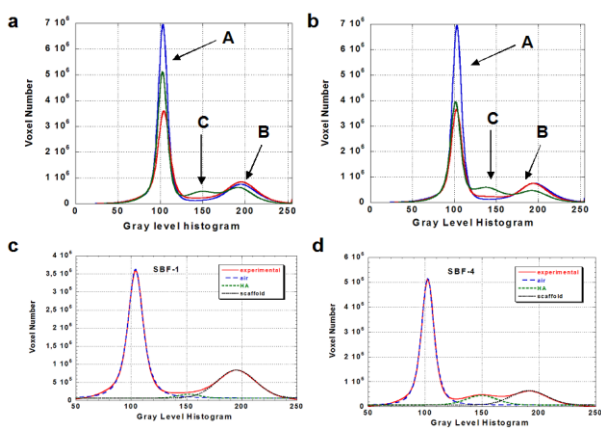
Figure 7. XRD spectra of the scaffolds before and after soaking in SBF (a) and TRIS (b): (A) before the treatment, (B) after 1 week, (C) after 4 weeks of immersion.
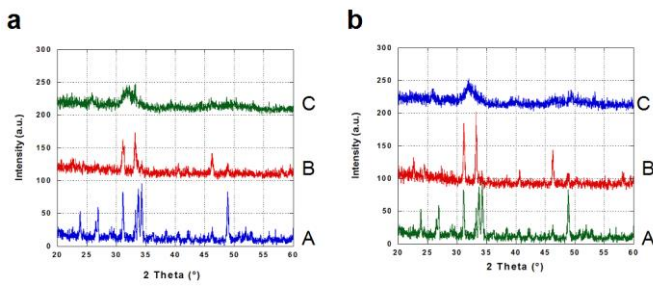

Figure 8. HAp layer formed on the pores scaffold surface after immersion in SBF for 28 days: (a) morphological and (b) back-scattered mode micrographs of a cross-section; (c) EDS analysis performed on HAp layer.
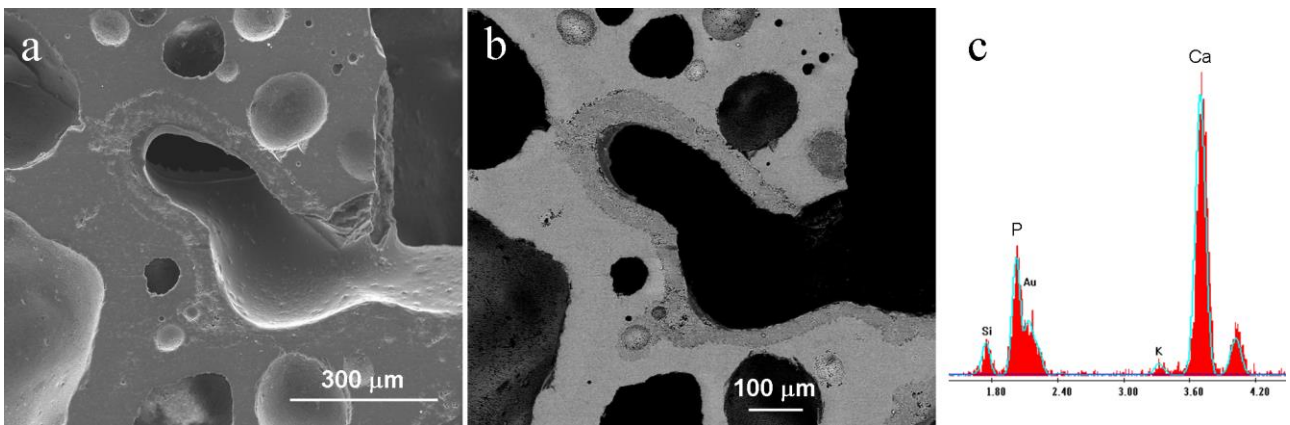
Figure 9. Example of a central virtual slice obtained by micro-CT with the material scaffolds (white) and the new phase (yellow): (a) slice of sample after treatment in SBF for 1 week and (b) for 4 weeks; image of the same slice after "cancelling" the scaffold material: (c) slice of sample after treatment in SBF for 1 week and (d) for 4 weeks.
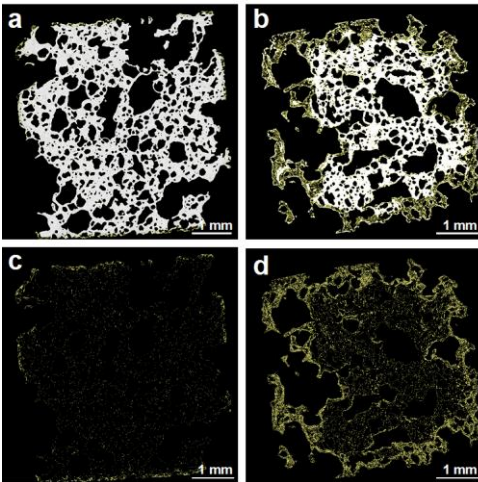
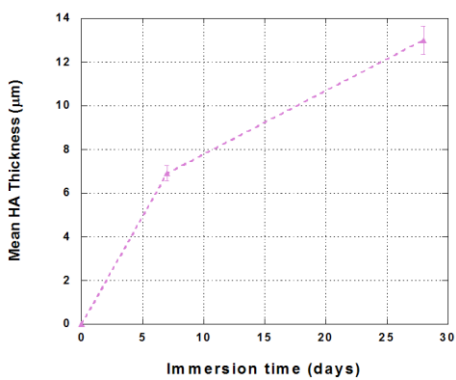Figure 10. Evolution of the new HAp thickness as a function of soaking time (samples in SBF).

Figure 11. Evolution of the mean trabeculae thickness as a function of soaking time (samples in TRIS).
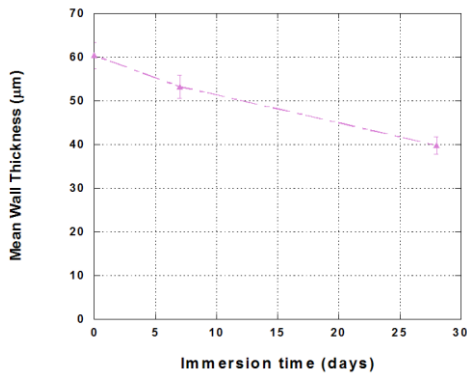

Figure 12. (a) Total porosity of the glass-ceramic scaffolds before (■) and after treatment in SBF for 1 week (■) and for 4 weeks (■); (b) pores size distribution of the glass-ceramic scaffolds before (■) and after treatment in TRIS for 1 week (■) and for 4 weeks (■).
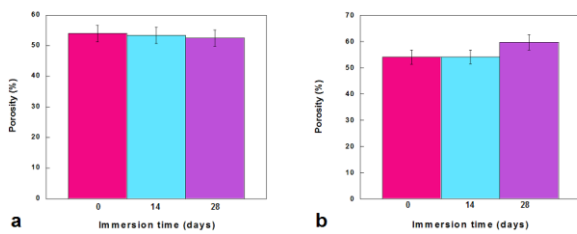

Figure 13. The 3D pore network showing the bimodal porous structure of the tissue-engineering scaffold as obtained by micro-CT.
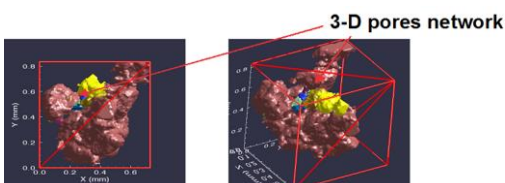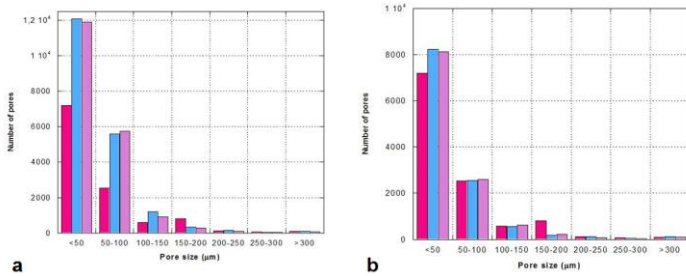
Figure 14. (a) Pore size distribution of the glass-ceramic scaffolds before (■) and after treatment in SBF for 1 week (■) and for 4 weeks (■); (b) pore size distribution of the glass-ceramic scaffolds before (■) and after treatment in a buffer (TRIS) for 1 week (■) and for 4 weeks (■).

Tables

Table 1. Summary of structural characteristics of highly porous glass-ceramic scaffolds.

Samples	(SV/TV)×100 (% vol.)	Porosity (1 − SV/VT)×100 (% vol.)	SS/SV	TbTh (μm)	TbSp (μm)
Glass-ceramic scaffolds	46.0±0.9	54.0±0.9	3.3±0.06	60.4±2.4	183.6±9.1
Glass-ceramic scaffolds after treatment in SBF for 1 week	46.6±0.9	53.4±0.9	3.7±0.07	55.4±1.1	124.6±6.2
Glass-ceramic scaffolds after treatment in SBF for 4 week	47.5±0.9	52.5±0.9	3.7±0.07	53.8±2.2	107.5±5.4
Glass-ceramic scaffolds after treatment in TRIS for 1 week	45.9±0.9	54.1±0.9	3.8±0.08	53.2±2.1	133.6±5.3
Glass-ceramic scaffolds after treatment in TRIS for 4 week	40.3±0.8	59.7±0.9	5.0±0.1	39.7±1.6	71.3±2.8